Beam-based sub-THz source at the CERN linac electron accelerator for research facility

A. Curcio,* M. Bergamaschi, R. Corsini, D. Gamba, W. Farabolini, T. Lefevre, and S. Mazzoni
CERN, CH-1211 Geneva 23, Switzerland

V. Dolci and M. Petrarca
Department of Basic and Applied Sciences for Engineering (SBAI) and INFN-Roma1, "Sapienza" University of Rome, Via A. Scarpa 14, 00161 Rome, Italy

S. Lupi
Physics Department of University of Rome "La Sapienza" and INFN-Roma1, Piazzale Aldo Moro 5, 00185 Rome, Italy

(Received 1 November 2018; published 4 February 2019)

We report on the radiation studies performed at the CLEAR facility of CERN in the sub-THz range, exploiting picosecond ultrarelativistic electron bunches for the production of coherent radiation. The coherent radiation, produced by different mechanisms (in particular coherent transition radiation), has been fully characterized using different techniques and detectors. The main aim has been that to setup a new beam-based source of radiation in the mm-waves for external users, individuating the performances and the limitations. Moreover the coherent radiation has been used for longitudinal diagnostics, providing reliable bunch length values consistent with other diagnostics. Transverse shaping of the radiation source has been also demonstrated via control of the size and divergence of the electron bunch at the source plane. The mechanism yielding the highest peak-power has been the Cherenkov-Diffraction Radiation, providing ~0.1 MW. The current performances of the CLEAR THz source seem to be more suitable for high-average-power than high-peak-power applications. Future plans and strategies will look toward the realization of a high-peak-power source, providing ~10–100 MW THz pulses.

DOI: 10.1103/PhysRevAccelBeams.22.020402

I. INTRODUCTION

Terahertz radiation, commonly addressed as the electromagnetic radiation within the range of frequencies 0.1–20THz (1 THz corresponding to 33 cm^{-1} wave number, 8 meV temperature and 300 mum wavelength), has a strong impact in many areas of research, from the time-resolved study of matter [1], to the quantum control of materials [2–5], to plasmonics [6–9], then tunable optical devices based on Dirac-electron systems [10], biological [11] and technological applications such as medical imaging [12] and security [13]. Striking applications for novel acceleration techniques exploiting high-intensity THz radiation have also been proposed and successfully tested [14–18]. Interest toward novel techniques of acceleration/deflection of particles driven by high intensity THz fields is rapidly growing within the scientific community and the race has started to the realization of sources with various performances all over the world. THz sources can normally be of two types: beam-based or laser-based. For beam-based is meant here a source which makes use of ultrashort ($\lesssim$1 ps) electron bunches for producing THz in the guise of coherent radiation. Another important kind of beam-based sources are free electron lasers [19–24], nevertheless not treated in this work. Laser-based sources are related to the optical rectification (or even to the difference frequency generation) of infrared pump lasers (fs) propagating through non-linear crystals [25]. Laser-based sources currently retain the primacy in terms of energy per pulse delivered, obtained by use of optical rectification of TW-class pump lasers in organic crystals, and therefore in terms of intensity and associated electric fields generated (up to 1 GV/m [26]). Also spectral and temporal shaping has been demonstrated in both laser-based and beam-based sources. Spectral and temporal shaping are two aspects which are intimately connected in this kind of THz radiation studies, due to the temporal coherence. Shaping by lasers is possible by acting on the temporal structure of the pump laser pulses [27,28], on their non-linear spectral phase [25] or even

*alessandro.curcio@cern.ch

exploring different kind of crystal compositions and size. Shaping by electron beams is performed by inducing modulations on the bunch structure at the picosecond level. This is feasible for photoinjectors via a previous shaping of the temporal structure of the photocathode laser pulse [27,28]. Energy per pulse of few tens μJ have been demonstrated by beam-based sources, when using electron bunches shorter than 1 ps and with a charge up to hundreds of pC, corresponding to high peak powers of the order of MW [27,28]. The CLEAR user facility at CERN hosts an electron LINAC (LINear ACcelerator) providing ps electron beams suitable for THz and sub-THz radiation studies. These kind of studies have been performed and the summary is reported in form of the present article. The performances of the source have been individuated and parameters for users have been determined. The uniqueness of the CLEAR system is the possibility to provide trains of hundreds of ps-bunches of many tens of pC charge with a repetition rate up to 10 Hz. This means high fluxes of sub-THz energy over time can be produced, as it has been experimentally observed. In particular the best performance of the CLEAR source has been ~0.1 MW peak power with energy ~400 μJ delivered per second as a train of 200 pulses of ps-duration. In brief, an average power of about half mW, peaked at 60 GHz with a relative bandwidth of 100%. The energy in a ~10 GHz bandwidth around 0.1 THz was around ~40 μJ, still interesting for THz applications. In particular, these kind of performances are quite attractive for spectroscopic and imaging applications, given the high integrated flux of energy achievable, as well as for testing various detectors and detection techniques. Applications in accelerator physics will require beam improvements in terms of charge per single bunch and single bunch duration in order to increase the peak power up to the hundreds of MW, at least. This is the goal for the next future. Meanwhile, different kind of sources have been explored based on different mechanisms of radiation, as coherent transition radiation (CTR), coherent diffraction radiation (CDR) and coherent Cherenkov-diffraction radiation (CChDR) [29–31]. The experimental comparison among different mechanisms in terms of peak power and energy per pulse has been made, showing that CChDR is more promising than the other mechanisms. Furthermore bunch length studies have been carried on, due to the synergy between coherent radiation and bunch form-factor, allowing for bunch length measurements. These tests have shown consistency between the coherent radiation-based longitudinal diagnostics and the other diagnostics along the accelerator beamline, as the rf-deflector and the streak-camera measurements of optical transition radiation (OTR). At least two techniques have been tested successfully, a standard one related to the direct retrieval of the bunch form-factor and another one exploiting the signal ratios at different frequencies. Finally, spatial and angular shaping of the radiation source has been verified by controlling the size and the divergence of the electron beam at the radiator plane. Future plans for the optimization of the performance of the CLEAR sub-THz source are object of discussion of Sec. VI. These will foresee the use of different radiators/radiation mechanisms as well as the improvement of the beam parameters, as the charge per single bunch and the shortness.

II. THE CLEAR FACILITY AT CERN

The CLEAR (Cern Linear Electron Accelerator for Research) facility is an electron LINAC machine, descending from a proposal to adapt and reuse CALIFES, the CTF3 (CLIC Test Facility) probe beam injector, as an electron injector for a new test beamline. The accelerator hall is approximately 42 m long and 7.8 m wide. The CLEAR beamline is composed of the CALIFES injector which is approximately 25 m long, followed by a 16 m-long beamline, as shown by Fig. 1.

The electron beam is generated on a Cs2Te photocathode (QE > 0.3%, lifetime 1 year) pulsed by an UV (converted from IR) laser [32,33]. The main laser parameters are summarized in Table I. The rf-gun, developed and built by LAL-Orsay [34], is followed by three LEP Injector Linac (LIL) [35,36] 4.5 m-long accelerating structures [37]. The first structure can be used to tune the bunch length from 0.5 ps to 10 ps rms. by means of velocity bunching. The gun, the buncher and first accelerating structure are immersed in a tunable solenoid field for focusing and space charge compensation. A matching section with three tunable quadrupoles and a spectrometer line complete the injector. CALIFES is equipped with a rich set of beam diagnostics [38]. In particular, bunch length measurements are possible by means of an electro-optical spectral decoding (EOSD) system [39], by streak camera measurements of OTR light [40], by using a dedicated S-Band RF deflector [41] or by detection of coherent radiation in the (sub-)THz range, which is one of the main topics of the present paper. The range of beam parameters obtainable at the end of CALIFES, and therefore available for users, are summarized

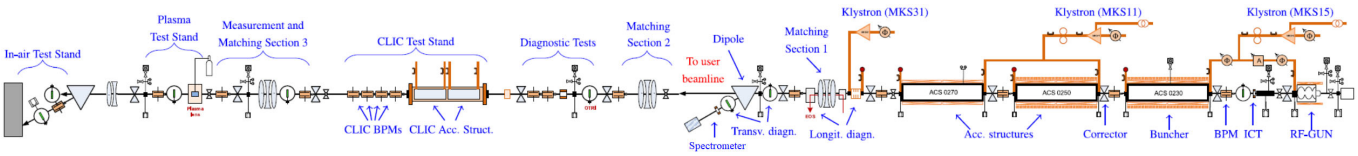

FIG. 1. The CLEAR beamline (from right to left).

TABLE I. Photo-injector laser parameters.

Laser parameter	Value range
Energy onto the cathode [nJ/pulse]	Up to ∼200
Intensity stability rms	$< 3\%$
Spot size onto the cathode FWHM [mm]	1
Pointing stability onto the cathode rms [mm]	< 0.2
Wavelength [nm]	262
Single pulse length FWHM [ps]	5
Frequency of the train of pulses [GHz]	1.5
Number of pulses in a train	Up to ∼200
Repetition rate [Hz]	0.833 to 10

TABLE II. Beam parameters at the end of CALIFES.

Beam parameter	Value range
Energy [MeV]	50 to 220
Bunch charge [nC]	0.001 to 1.5
Norm. emittance [μm]	∼5
Bunch length rms [ps]	0.5 to ∼10
Relative energy spread rms	$< 0.2\%$
Frequency of the train of bunches [GHz]	1.5
Number of bunches in a train	Up to ∼200
Repetition rate [Hz]	0.833 to 10

in Table II. The straight line ends about 20m after the first spectrometer with a 100 μm thick aluminium window, leaving ∼1.5 m long in-air path for the beam. This area presently hosts the sub-THz radiation studies.

III. SPECTRAL-ANGULAR CHARACTERIZATION OF THE CTR SOURCE

In this section we show the spectral-angular studies of sub-THz radiation produced as coherent transition radiation. A full characterization of this kind has been useful for different reasons. For example, as discussed in Sec. IV, knowing the angular distribution of the radiation, in particular in the prewave zone, allows the determination of the bunch length by use of a complete set of Schottky diodes covering a range of frequencies from few tens to a few hundreds of GHz. Also the determination of the source size and of the angular distribution in the far field is fundamental information for possible users of this radiation source. We exploited two different setups, as shown by Fig. 2. In the first setup the electron beam passed trough the radiator, then the radiation was reflected back to the detector, a Schottky diode (or a set of diodes) coupled to a waveguide band-pass filter plus a gain-horn. Prewave zone measurements were possible in this configuration. The angular scan of the p-polarization was made. In the second setup the electron beam passed trough the radiator, then the radiation was collected/focused by an off-axis-parabola, filtered by means of a band-pass-filter, finally

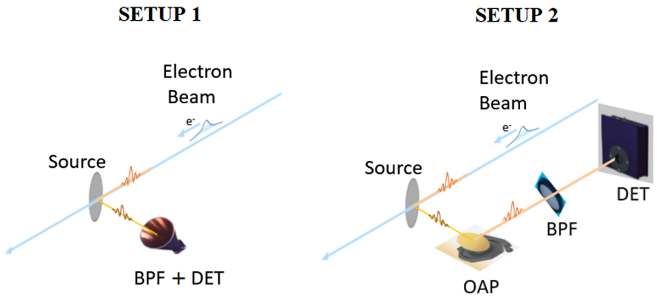

FIG. 2. Setup 1: the electron beam e^- (blue line) passes trough the radiator, then the radiation (orange line) is reflected back to the detector (DET), a Schottky diode coupled to a waveguide BPF plus a gain-horn. Prewave zone measurements are possible. The angular scan of the p-polarization is made. Setup 2: the electron beam e^- (blue line) passes trough the radiator, then the radiation (orange line) is collected/focused by an off-axis-parabola (OAP), it is filtered by means of a band-pass-filter (BPF), finally reaches the detector (DET), in this case a THz camera. Both far-field and near-field measurements are possible, adjusting the relative position between the parabola and the camera and/or the relative distance between the parabola and the radiator.

reaching the detector, in this case a THz pyrocamera or a pyroelectric sensor. Both far-field and near-field measurements were possible, adjusting the relative position between the parabola and the camera and/or the relative distance between the parabola and the radiator.

The first results of spectral-angular characterization were obtained by exploiting the first setup. The p-polarization of the CTR radiation was studied in terms of its angular distribution by rotating the radiator (an Al-coated screen, 200 μm thick, 10 cm diameter) along its principal axis in order to scan the angular distribution at the detector plane. The distributions obtained were then automatically deconvoluted with the angular aperture of the detector, in order to eliminate spurious contributions, more related to the detection apparatus than to the source itself. The frequencies studied with the zero-biased Schottky diodes fell in different ranges, i.e., 0.071–0.073 THz, then 0.09–0.14 THz, 0.14–0.22 THz and 0.22–0.33 THz (see Fig. 3). For doing the angular scans the diodes have been used one by one, with the possibility to insert and align one or another by means of suitable optomechanics. The distance between the radiator and the diodes was 30 cm. Since the field of the electron bunch, responsible for the radiation mechanism through electric polarization of the radiator surface, had an extension $\gamma\lambda$ (where $\gamma \sim 430$ is the Lorentz factor for 215 MeV electrons), much greater than the radiator radius $a = 5$ cm, diffractive effects were dominating. The far-field zone in this configuration is calculated by diffraction theory, and it corresponds to one Rayleigh length $\pi a^2/\lambda$. For $\lambda \sim 3$ mm (corresponding to 0.1 THz) the Rayleigh length is greater than 2 m, in turn much greater than 30 cm, therefore the condition of prewave zone

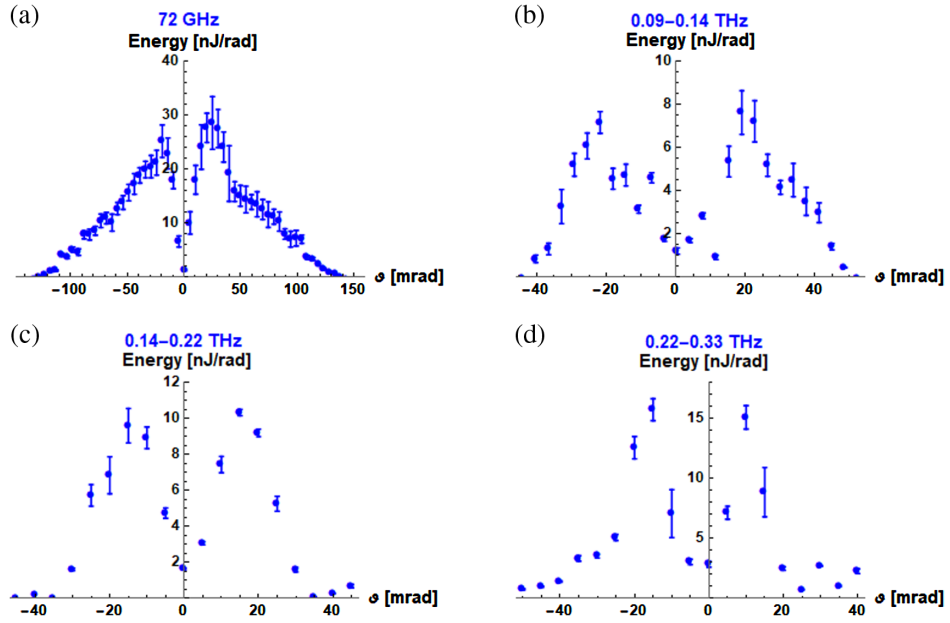

FIG. 3. Profiles of far-field CTR (p-polarization) measured at different frequencies: 72 GHz (a), 90–140 GHz (b), 0.14–0.22 THz (c), 0.22–0.33 THz (d). Electron beam parameters (per single bunch): 215 MeV, 1.5 ps, 40 pC.

was encountered in the detection of this wavelength. Figure 4 also puts into evidence the transition between the prewave zone towards the far-field, since the distance between the radiation lobes narrows and approaches to a constant value. This means that the frequencies for which the prewave condition stops holding strongly are emitted approximately within the same angular aperture. The far-field condition is fully verified when all the frequencies, are emitted within the same lobe aperture. In fact, for wavelengths such that $\lambda \ll a$ the far field condition is not anymore dictated by diffraction (Rayleigh length), but, since backward radiation is here considered, the far-field zone is reached after a distance comparable to the wavelength itself. The comparison with simulations, in Fig. 5, gave good agreement in terms of the distances between the main lobes and in the scale of transition between the prewave zone and the far-field zone. The slight disagreement at frequencies below 0.1 THz in terms of lobe-width was only an artefact of the smoothing algorithm used for producing Fig. 4. During this study particular attention was payed also on the quantitative determination of the radiated energy, about 60 nJ, and of the peak power delivered, about 40 kW. These parameters referred to standard beam parameters (per single bunch): 215 MeV, 1.5 ps, 40 pC. This information shall be fundamental for possible users of (sub-)THz at CLEAR and especially to understand in which way to improve the CLEAR beam parameters to get better performances of the source itself. The second setup shown in Fig. 2 was exploited for doing the imaging of the CTR source (near-field measurements) and also, remotely controlling the optics, for characterizing the angular distribution of the CTR source in the far-field.

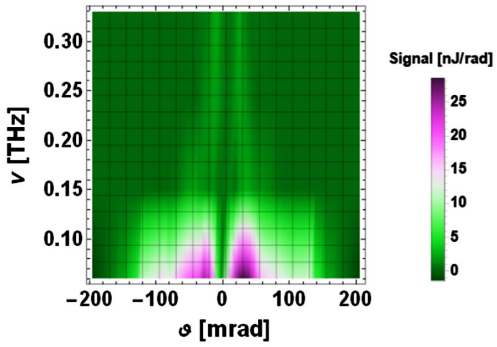

FIG. 4. Smoothed representation of the experimental results on spectral-angular characterization of the CTR light emitted by a 215 MeV, 40 pC, 1.5 ps long electron bunch at 30 cm from the source.

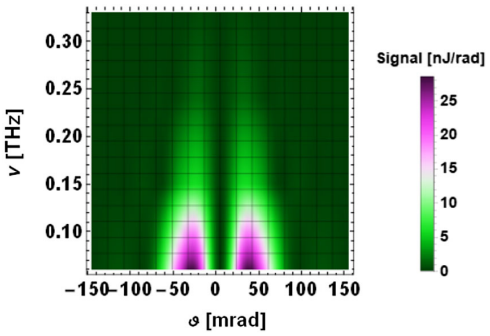

FIG. 5. Simulation of spectral-angular characterization of the CTR light emitted by a 215 MeV, 40 pC, 1.5 ps long electron bunch in the prewave zone at a distance 30 cm.

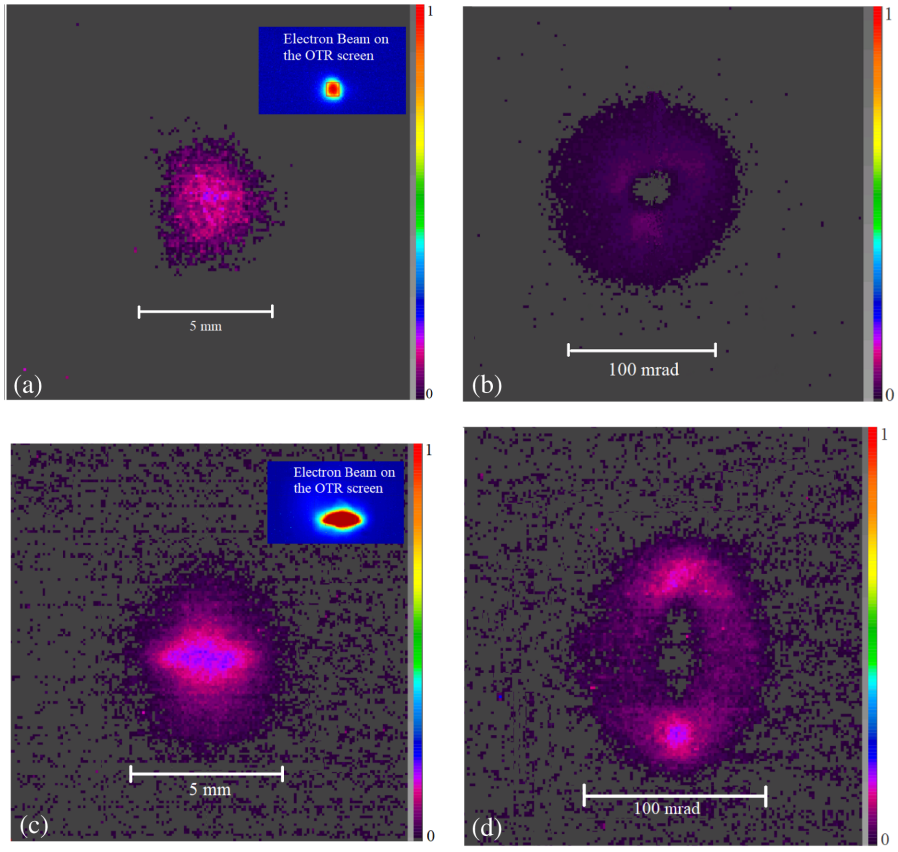

FIG. 6. Far field and near field images (color palette in arbitrary units) of CTR over the whole spectral range of emission. Images (a) and (b) show the near and far field CTR distribution, respectively, for a symmetric round electron bunch. Images (c) and (d) show the near and far field CTR distribution, respectively, for an asymmetric electron bunch, demonstrating the possibility to control the energy distribution of the radiation both in near and far field via a transverse shaping of the bunch (size and divergence at the source plane). Electron beam parameters (per single bunch): 215 MeV, 1.5 ps, 40 pC.

These studies were clearly possible with the help of a focusing optics, an off-axis parabola as already mentioned. Figure 6 shows images of the CTR source and its angular distribution over the whole spectral range of emission, i.e., without any band-pass filter in front of the camera. Images of the upper row show the near and far field CTR distribution, respectively, for a symmetric round electron bunch. Images of the lower row show the near and far field CTR distribution, respectively, for an asymmetric electron bunch, demonstrating the possibility to control the energy distribution of the radiation both in near and far field via a transverse shaping of the bunch (size and divergence) at the source plane. The electron beam parameters (per single bunch) for this study were again 215 MeV of energy, 1.5 ps the time duration and 40 pC the charge.

IV. BUNCH LENGTH DIAGNOSTICS

One of the first applications of coherent radiation at CLEAR, in particular coherent transition radiation, was the bunch length diagnostics. In fact, all the other longitudinal diagnostics are placed upstream along the beamline of the accelerator and having further diagnostics at the end of the straight line before the last dump on the "in-air test-stand" (Fig. 1) could be of great advantage for experiments in that area. The strategy for bunch length diagnostics was that to install a complete set of Schottky diodes, some of them coupled to waveguide band-pass filters and each of them coupled to gain-horns, covering a whole range of frequencies from 26.5–300 GHz. The installation was exploited as a (sub-)THz spectrometer for the longitudinal diagnostics of the CLEAR electron bunches. This kind of experiment referred to the Setup 1 in Fig. 2. Simultaneously, bunch compression studies started, with the achievement of bunch length compression down to few hundreds of femtoseconds rms via velocity bunching. The bunch length compression during these first tests was made only by varying the gun phase in order to ease the beam transport along the accelerator without changing any other parameter. This allowed a direct comparison among the different diagnostics, placed at different points of the beamline. The Schottky diodes operating at higher frequencies (~0.1–0.3 THz) where not used for making CTR spectroscopy or in general to retrieve the bunch length, nevertheless they showed to be

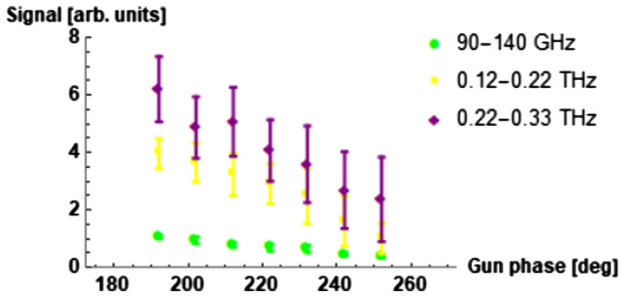

FIG. 7. Signature of the bunch compression versus the gun phase, recorded for different ranges of frequency in the sub-THz domain. When the bunch length is shortened from many ps down to $\lesssim$1 ps, the "high"-frequency Schottky diodes detect greater signals of coherent radiation.

useful monitors of bunch length compression, as described by Fig. 7. The signal were processed for taking into account the different relative sensitivities among the detectors and also for the different solid angle of collection. The difference in the absolute signal level among the detectors had also to be related to the different bandwidths that the detectors were able to collect. When the bunch length was shortened from many ps down to $\lesssim$1 ps, these diodes were detecting greater signals of coherent radiation accordingly. The sub-THz spectrometer was used to characterize such short bunches and it demonstrated to be working fine in the range of bunch length 0.8–4 ps. The low limit being determined by the poorer charge (between 1–10 pC) transported down to the dump when compressing the bunch length only varying the gun-phase and the upper limit given by the limited availability of waveguide band-pass filters in the few tens of GHz region. One example of CTR spectrum detected and compared to simulations is given by Fig. 8 for a ~3 ps long bunch. The validity of the bunch length measurements with such a device was corroborated by the simultaneous use of different longitudinal diagnostic devices, like the rf deflector and the optical streak-camera, streaking OTR light, as shown by Fig. 9. The radiation formulas used for the simulations

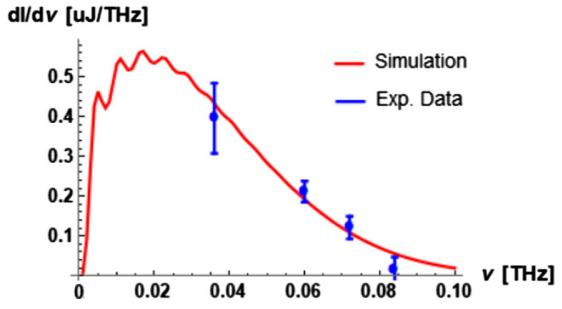

FIG. 8. CTR spectrum, comparison between simulations and experimental data for a bunch length of approximately 3 ± 0.5 ps. Oscillations at low frequencies are due to interference effects related to the finite-size of the radiator [42]. Electron beam parameters (per single bunch): 215 MeV, 3 ps, 40 pC.

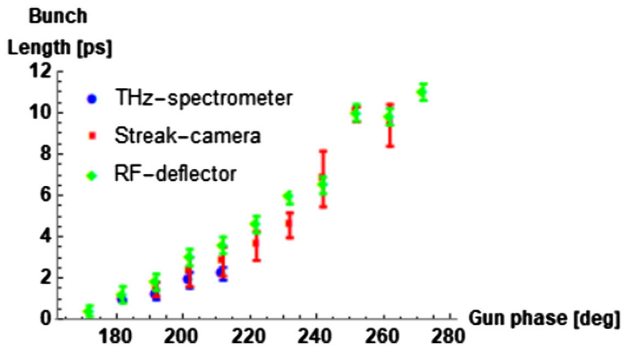

FIG. 9. Bunch length measurements with different techniques/detectors. The bunch length compression in this case was made only by varying the gun phase in order to ease the beam transport along the accelerator without changing any other parameter. This allowed a direct comparison among the different diagnostics, placed at different points of the beamline. A full range 0.5 ps to ~10 ps has been demonstrated.

were Eqs. (1) and (2), taking into account for the single-particle emission intensity I_{sp} with diffractive/near-field corrections [42]. Notice that the nonlinear phase factor in Eq. (1) approaches to zero for $R \gg \lambda$, i.e., for long distances R of detection.

$$\frac{dI_{\mathrm{sp}}^2}{d\Omega d\omega} = C\left|\int_0^a J_1(k\rho\sin\theta)K_1\left(\frac{k\rho}{\beta\gamma}\right)\exp\frac{ik\rho^2}{2R}\right)\rho d\rho\Big|^2 \tag{1}$$

$$C = \frac{e^2\omega^4}{4\pi^3\varepsilon_0 c^5\beta^4\gamma^2} \tag{2}$$

$$e^{-(\omega_1^2-\omega_2^2)\sigma_\tau^2}\frac{\frac{dI_{\mathrm{sp}}^2}{d\Omega d\omega}(\omega_1,\Omega_1)}{\frac{dI_{\mathrm{sp}}^2}{d\Omega d\omega}(\omega_2,\Omega_2)} = \frac{S_1(\omega_1,\Omega_1)}{S_2(\omega_2,\Omega_2)} \tag{3}$$

$$\sigma_\tau = \sqrt{\left|\frac{1}{\omega_1^2-\omega_2^2}\log\left\{\frac{\frac{dI_{\mathrm{sp}}^2}{d\Omega d\omega}(\omega_2,\Omega_2)S_1(\omega_1,\Omega_1)}{\frac{dI_{\mathrm{sp}}^2}{d\Omega d\omega}(\omega_1,\Omega_1)S_2(\omega_2,\Omega_2)}\right\}\right|} \tag{4}$$

The quantities appearing in Eq. (1) are the elementary charge e, the electromagnetic pulsation ω, related to the electromagnetic frequency ν through $\omega = 2\pi\nu$. The dielectric constant of vacuum is ε_0, the velocity of light in vacuum is, as standard, c. The normalized velocity of the electron is $\beta = \sqrt{1-1/\gamma^2}$. The wave number is $k = \omega/c = 2\pi/\lambda$. The Bessel function of first kind of order n are denoted by the capital letter J_n, while the Bessel of second kind are K_n. Finally the angle θ is the polar angle of emission. Equation (1) describes the incoherent part of emission, which, over the whole bunch of electrons, scales as the bunch charge. Furthermore, except for corrections at low frequency due to the finite-size of the radiator and at large frequencies comparable to the plasma frequency of the radiator, it exhibits a flat white spectrum. On the other hand

the coherent part of the radiation spectrum is obtained multiplying Eq. (1) by the squared number of electrons within the emitting bunch and by the so-called form-factor, related to the temporal shape of the bunch. For a Gaussian bunch the form-factor is $\exp(-\omega^2\sigma_\tau^2)/2\pi$, where σ_τ is the rms bunch duration, measured on the current density profile. The bunch length measurement through CTR radiation at CLEAR have been performed following two different methods. The first method, referring to the experimental results of Fig. 8, was that of (sub-)THz spectroscopy of CTR light. The frequency studied in this case where 36 ± 1 GHz, 60 ± 1 GHz, 72 ± 1 GHz and 84 ± 1 GHz. This was accomplished with a set of Schottky diodes placed at the same polar positions, characterized with high-precision in order to compare the different signals at the same time using the results shown in Sec. III. The measurements where recorded for a round bunch transverse shape with a rms size $\sigma_r \lesssim 1$ mm. This method offered the possibility to experimentally retrieve part of the bunch form-factor, and then comparing with simulations for a Gaussian bunch, the best fit was used to extrapolate the bunch length. A more complete measurement of the bunch form-factor would have required the possibility to detect radiation in the range of few tens of GHz. This was not possible according to our availability of detectors, therefore the assumption of Gaussian bunch was necessary for doing a comparison and a best fit yielding a bunch length value. Nevertheless the Gaussian-shape of the bunch was verified by means of the rf-deflector measurements and also the streak-camera measurements. The second method adopted, still based on the assumption of Gaussian bunch was related to the Eqs. (3) and (4). Indeed, Eq. (3) tells that the ratio between the radiation intensity S collected in correspondence of two different frequencies within two different solid angles (like in the setup with a whole set of Schottky diodes used as a spectrometer) is proportional to the ratio of the incoherent single-particle emission intensities times a function F related to the bunch form-factor. The inversion of Eq. (3) gives an expression for the bunch length σ_τ, as prescribed by Eq. (4). Corrections to σ_τ in Eq. (4) due to the beam size σ_r at the detector plane are of the order $\sigma_r/\gamma c$, negligible in our case where $\sigma_r \lesssim 1$ mm. Both the two methods showed to be reliable and consistent. The spectrum of Fig. 8 was recorded for a gun-phase ~210°, perfectly in agreement with the multiple-diagnostics scan of Fig. 9. Moreover the experimental points of Fig. 9 concerning the THz spectrometer have been retrieved by applying the second method, i.e., by use of the ratio between different couples of signals, then implementing Eq. (3) and (4). The advantage of the second method over the first one was that to have the possibility to detect bunch lengths much shorter than ~2 ps, down to ~0.8 ps (Fig. 9). This was not possible with the sub-THz spectrometer because the highest frequencies which could be studied with that device fell below 0.1 THz, corresponding in terms of bunch form-factor to a minimum bunch length detectable $\gtrsim 2$ ps.

V. COMPARISON AMONG DIFFERENT RADIATION MECHANISMS

Summarizing the performances of the CTR source presented in Secs. III and IV, the best performance of the CLEAR CTR source was ~40 kW peak power with energy ~120 μJ delivered per second as a train of 200 pulses of ps-duration. Such performance was obtained by using the following electron beam parameters (per single bunch): 215 MeV, 1.5 ps, 40 pC. These parameters, recurrent all through the present article, consisted in a stable working point for the CLEAR machine, being a compromise between the transport of relatively high-charge per single bunch (~70–80% of the total at the gun) down to the THz in-air test-stand, and bunch compression accomplished with variations of the sole gun-phase towards the ps-level. Beside the characterization of the CTR source, further studies were carried on in order to determine whether or not, and especially in which terms, different radiation mechanisms could provide higher performances. The two other mechanisms explored were the coherent diffraction radiation (CDR) and the coherent Cherenkov-diffraction radiation (CChDR). The CDR radiator was a Al disk 200 μm thick with a hole in the center, the external diameter being 10 cm, while the internal 0.5 cm. The Cherenkov-diffraction radiator (made by teflon) was 5.4 cm long with 5 cm base diameter, designed with a 5 mm diameter hollow channel along the symmetry axis.

Spectroscopic measurements of the kind explained in Secs. III and IV (related to the Setup 1 of Fig. 2), detecting the spectral power at different wavelengths, allowed the comparison among the CDR, CTR, and CChDR radiation mechanisms. The CDR mechanism revealed to provide pretty similar performances than CTR, as shown in Table III. This was due to the fact that the cutoff frequency, due to the hole in the middle of the CDR radiator, was ~4 THz. The cut-off frequency is the frequency which cannot be produced since the bunch field (at that frequency) does not reach the edge of the internal hole of the radiator, therefore not polarizing the surface atoms for emitting radiation. Since the coherence band, related to the bunch form-factor was not extending sensitively above 0.1 THz, the hole in the middle played only the role of decreasing by few percent the amount of radiated power, not affecting the radiation spectrum. Moreover, the yield of coherent radiation by a 5 cm long Cherenkov radiator was studied by inserting it along the electron beam path and then using the CTR screen as a mirror for extracting the radiation out to the detector. The teflon Cherenkov cone was cut in such a way to build a forward plane-wave of radiation, copropagating with the beam towards the mirror. A significant enhancement of about a factor 3 higher in photon yield with respect to a CTR/CDR radiator was observed at a radiator-mirror distance of about 40 cm as well as a slight shift towards a higher peak frequency (proper of the Cherenkov mechanism itself), consistent with the observations in [43]. An average power of about half mW, peaked at 60 GHz

TABLE III. Parameters of the CLEAR sub-THz source for the following electron beam parameters (per single bunch): 215 MeV, 1.5 ps, 40 pC.

Radiation mechanism: CTR	
Peak Power [kW]	$\sim 40 \pm 3$
Average Power [mW]	$\sim 0.13 \pm 0.01$
Energy per pulse [nJ]	$\sim 60 \pm 5$
Energy per train of 200 pulses [μJ]	$\sim 12 \pm 1$
Peak frequency [GHz]	~ 40
Bandwidth [GHz]	~ 40
Energy per pulse at 0.1 THz [nJ]	$\sim 6 \pm 0.5$
Energy per train of 200 pulses at 0.1 THz [μJ]	$\sim 1.2 \pm 0.1$
Radiation mechanism: CDR	
Peak Power [kW]	$\sim 35 \pm 3$
Average Power [mW]	$\sim 0.11 \pm 0.01$
Energy per pulse [nJ]	$\sim 53 \pm 5$
Energy per train of 200 pulses [μJ]	$\sim 10.6 \pm 1.1$
Peak frequency [GHz]	~ 40
Bandwidth [GHz]	~ 40
Energy per pulse at 0.1 THz [nJ]	$\sim 5.3 \pm 0.5$
Energy per train of 200 pulses at 0.1 THz [μJ]	$\sim 1.1 \pm 0.1$
Radiation mechanism: CChDR	
Peak Power [MW]	$\sim 0.12 \pm 0.01$
Average Power [mW]	$\sim 0.38 \pm 0.04$
Energy per pulse [nJ]	$\sim 190 \pm 20$
Energy per train of 200 pulses [μJ]	$\sim 38 \pm 4$
Peak frequency [GHz]	~ 60
Bandwidth [GHz]	~ 60
Energy per pulse at 0.1 THz [nJ]	$\sim 19 \pm 2$
Energy per train of 200 pulses at 0.1 THz [μJ]	$\sim 3.8 \pm 0.4$

with a relative bandwidth of 100% was obtained finally. The energy in a ∼10 GHz bandwidth around 0.1 THz was around 10% of the total. A complete spectral-angular characterization, especially for the CChDR source of the kind demonstrated in Sec. III, as well as bunch length-diagnostics based on the Cherenkov-diffraction mechanism will be the interest of new detailed study of next future at CLEAR. Meanwhile, the graphic representation comparing the peak powers measured for the different radiation mechanisms analyzed is reported in Fig. 10.

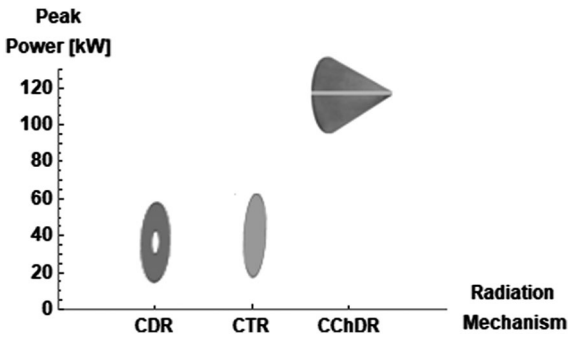

FIG. 10. Peak power of the CLEAR sub-THz source for the following electron beam parameters (per single bunch): 215 MeV, 1.5 ps, 40 pC. The experimental points have been represented by the sketch of the radiators corresponding to the different radiation mechanisms explored.

VI. CONCLUSIONS AND PERSPECTIVES

In this paper we have shown the experimental studies on sub-THz radiation performed at the CERN facility CLEAR. The motivation for these studies was that to understand performances and limits with the current parameters of the machine, thus individuating actual parameters of a source for external users. The uniqueness of the CLEAR system is the possibility to provide trains of hundreds of ps-bunches of many tens of pC charge with a repetition rate up to 10 Hz. This means high fluxes of sub-THz energy over time can be produced, as it has been experimentally observed. The best performance of the CLEAR source has been ∼0.1 MW peak power with energy ∼400 μJ delivered per second as a train of 200 pulses of ps-duration. An average power of about half mW, peaked at 60 GHz with a relative bandwidth of 100% has been obtained. The energy in a ∼10 GHz bandwidth around 0.1 THz has been ∼40 μJ. According to our calculations, based on the Planck formula, an average power emitted like 0.5 mW would require a source temperature comparable to the normal room temperature. Nevertheless the black body source is typically a continuous-wave source and with isotropic emission. On the contrary, a source based on coherent radiation by relativistic electron bunches is directional and therefore much more brilliant. Furthermore, the average power is surely an interesting parameter by which the source can be described, but this parameter hides the fact that the source presents a characteristic time structure related to the photocathode-laser and the RF systems. The CLEAR-based source is indeed a pulsed source. Summarizing, the intensity of a beam-based source is order of magnitudes higher than the one proper of a black-body source. Considering the CLEAR-source, hundreds of $\lesssim$ps pulses can be used to probe samples down to that time scale, and this experiment can be repeated up to a rate of 10 Hz. With a suitable temporal shaping of the photocathode-laser pulse, to be performed in the next future, it will be possible even to tune the radiation spectrum on specific harmonics. Finally, the use of the Cherenkov-diffraction mechanism, as demonstrated in this paper, can be even more convenient than the transition/diffraction radiation in terms of power and directionality. Plans for the future are manifold. First of all we would like to better test long radiators for the Cherenkov-diffraction mechanism, as well it could be worthy to investigate other radiation mechanisms, still exploiting long radiators, like long gratings for coherent Smith-Purcell radiation (CSPR). We would like to further demonstrate the advantage and the limits of using long radiators for increasing the energy and/or the peak power of radiation emitted in the sub-THz range. Then we would like to improve our technique of bunch length diagnostics, for

example testing a Cherenkov-diffraction-based device instead then a CTR source, suffering of angular distribution issues. Finally we would like to reach peak power of coherent radiation in the sub-THz range of at least 1–10 MW. This can be accomplished by pushing the beam parameters to 0.5 ps bunch length and 100 pC bunch charge, affordable for the CLEAR machine in the next future. The final goal, for competitive applications like electron deflection or even acceleration/deceleration, would be to reach peak powers for coherent radiation in the range of the hundreds MW. Many hundreds of pC per single bunch and ∼100 fs bunch lengths will be needed for this task, but also understanding which is the best strategy in terms of radiation production, i.e., which is the best radiator/mechanism to be exploited. All the studies performed and presented here fall within this framework of projects and ideas.

[1] Workshop on Terahertz Sources for Time Resolved Studies of Matter, 2012, Argonne National Laboratory, Argonne, IL, USA.

[2] M. Rini, R. Tobey, N. Dean, J. Itatani, Y. Tomioka, Y. Tokura, R. W. Schoenlein, and A. Cavalleri, Control of the electronic phase of a manganite by mode-selective vibrational excitation, Nature (London) **449**, 72 (2007).

[3] A. Rostami, H. Rasooli, and H. Baghban, *Terahertz Technology: Fundamentals and Applications* (Springer Science & Business Media, New York, 2010).

[4] X.-C. Zhang and J. Xu, *Introduction to THz Wave Photonics* (Springer, New York, 2010).

[5] *Handbook of Terahertz Technologies: Devices and Applications*, edited by H. J. Song and T. Nagatsuma (CRC Press, Pan Stanford, 2015).

[6] A. Toma, Squeezing terahertz light into nanovolumes: Nanoantenna enhanced terahertz spectroscopy (NETS) of semiconductor quantum dots, Nano Lett. **15**, 386 (2014).

[7] P. Di Pietro *et al.*, Observation of Dirac plasmons in a topological insulator, Nat. Nanotechnol. **8**, 556 (2013).

[8] F. D'Apuzzo, A. R. Piacenti, F. Giorgianni, M. Autore, M. C. Guidi, A. Marcelli, U. Schade, Y. Ito, M. Chen, and S. Lupi, Terahertz and mid-infrared plasmons in three-dimensional nanoporous graphene, Nat. Commun. **8**, 14885 (2017).

[9] O. Limaj, F. Giorgianni, A. Di Gaspare, V. Giliberti, G. de Marzi, P. Roy, M. Ortolani, X. Xi, D. Cunnane, and S. Lupi, Superconductivity-induced transparency in terahertz metamaterials, ACS Photonics **1**, 570 (2014).

[10] F. Giorgianni *et al.*, Strong nonlinear terahertz response induced by Dirac surface states in Bi2Se3 topological insulator, Nat. Commun. **7**, 11421 (2016).

[11] THz Bridge-Tera-Hertz radiation in Biological Research, Investigation on Diagnostics and study of potential Genotoxic Effects, http://www.frascati.enea.it/THz-BRIDGE/.

[12] E. Pickwell and V. P. Wallace, Biomedical applications of terahertz technology, J. Phys. D **39**, R301 (2006).

[13] TeraHertz for Defence and Security, *A Defence Science Technology Office workshop at the frontier of technology, 2004, Adelaide, Australia*, http://www.eleceng.adelaide.edu.au/thz/program.htm.

[14] E. A. Nanni, W. R. Huang, K.-H. Hong, K. Ravi, A. Fallahi, G. Moriena, R. J. Dwayne Miller, and F. X. Kärtner, Terahertz-driven linear electron acceleration, Nat. Commun. **6**, 8486 (2015).

[15] L. Wimmer, G. Herink, D. R. Solli, S. V. Yalunin, K. E. Echternkamp, and C. Ropers, Terahertz control of nanotip photoemission, Nat. Phys. **10**, 432 (2014).

[16] W. R. Huang, A. Fallahi, X. Wu, H. Cankaya, A.-L. Calendron, K. Ravi, D. Zhang, E. A. Nanni, K.-H. Hong, and F. X. Kärtner, Terahertz-driven, all-optical electron gun, Optica **3**, 1209 (2016).

[17] C. Kealhofer, W. Schneider, D. Ehberger, A. Ryabov, F. Krausz, and P. Baum, All-optical control and metrology of electron pulses, Science **352**, 429 (2016).

[18] A. Curcio, A. Marocchino, V. Dolci, S. Lupi, and M. Petrarca, Resonant plasma excitation by single-cycle THz pulses, Sci. Rep. **8**, 1052 (2018).

[19] J. W. J. Verschuur, G. J. Ernst, B. M. van Oerle, D. Bisero, A. F. M. Boumanb, and W. J. Wittemana, Lasing experiments at TEUFEL, Nucl. Instrum. Methods Phys. Res., Sect. A **393**, 197 (1997) .

[20] D. Oepts, A. van der Meer, and P. van Amersfoort, The free-electron-laser user facility FELIX, Infrared Phys. Technol. **36**, 297 (1995).

[21] A. K. Freund, H. P. Freund, and M. R. HowellsCoherent electron-beam x-ray sources: Techniques and applications, Proc. SPIE Int. Soc. Opt. Eng. **3154**, 144 (1997).

[22] G. P. Gallerano and S. G. Biedron, Overview of terahertz radiation sources, in *Proceedings of the 2004 Free-Electron Laser Conference* (2004), www.JACoW.org, FRBIS02, p. 216.

[23] S. G. Biedron, J. W. Lewellen, S. V. Milton, N. S. Gopalsami, J. Schneider, L. Skubal, Y. Li, M. Virgo, G. P. Gallerano, A. Doria, E. Giovenale, G. Messina, and I. Panov Spassovsky, Compact, high-power electron beam based terahertz sources, Proc. IEEE **95**, 1666 (2007) and a related patent application by Biedron *et al.*

[24] FEL conference 2012: https://accelconf.web.cern.ch/AccelConf/FEL2012/html/auth0839.htm.

[25] A. Curcio, V. Dolci, S. Lupi, and M. Petrarca, Terahertz-based retrieval of the spectral phase and amplitude of ultrashort laser pulses, Opt. Lett. **43**, 783 (2018).

[26] C. Vicario, B. Monoszlai, and C. P. Hauri, GV/m Single-Cycle Terahertz Fields from a Laser-Driven Large-Size Partitioned Organic Crystal, Phys. Rev. Lett. **112**, 213901 (2014).

[27] E. Chiadroni *et al.*, The SPARC linear accelerator based terahertz source, Appl. Phys. Lett. **102**, 094101 (2013).

[28] E. Chiadroni *et al.*, Characterization of the THz radiation source at the Frascati linear accelerator, Rev. Sci. Instrum. **84**, 022703 (2013).

[29] D. V. Karlovets and A. P. Potylitsyn, Universal description for different types of polarization radiation, arXiv:0908.2336.

[30] R. Kieffer, L. Bartnik, M. Bergamaschi, V. V. Bleko, M. Billing, L. Bobb, and R. O. Jones, Direct Observation of Incoherent Cherenkov Diffraction Radiation in the Visible Range, Phys. Rev. Lett. **121**, 054802 (2018).

[31] A. Curcio, M. Anania, F. Bisesto, M. Botton, M. Castellano, E. Chiadroni, and Z. Henis, Electro-Optical Detection of Coherent Radiation Induced by Relativistic Electron Bunches in the Near and Far Fields, Phys. Rev. Applied **9**, 024004 (2018).

[32] I. N. Ross, Feasibility study for the CERN CLIC photo-injector laser system, in CERN Technical Report No. CLIC-Note-462, 2000.

[33] M. Petrarca, H. H. Braun, E. Chevallay, S. Doebert, K. Elsener, V. Fedosseev, G. Geschonke, R. Losito, A. Masi, O. Mete, L. Rinolfi, A. Dabrowski, M. Divall, N. Champault, G. Bienvenu, M. Jore, B. M. Mercier, C. Prevost, R. Roux, and C. Vicario, First results from commissioning of the phin photo injector for CTF3, in *Proceedings of the 23rd Particle Accelerator Conference, Vancouver, Canada, 2009* (IEEE, Piscataway, NJ, 2009), p. MO6RFP063.

[34] J. Brossard, M. Desmons, B. M. Mercier, C. P. Prevost, and R. Roux, Construction of the probe beam photo-injector of CTF3, in *Proceedings of the 10th European Particle Accelerator Conference, Edinburgh, Scotland, 2006* (EPS-AG, Edinburgh, Scotland, 2006), pp. 828–830.

[35] R. Bossart, J. P. Delahaye, J. C. Godot, J. H. B. Madsen, P. Pearce, A. J. Riche, and L. Rinolfi, The LEP injector linac, CERN Technical Report No. CERN-PS-90-56-LP, 1990.

[36] LEP Injector Study Group, LEP design report, Vol I. *The LEP Injector Chain* (CERN, Geneva, Switzerland, 1983).

[37] G. Bienvenu, J. C. Bourdon, P. Brunet, and J. Rodier, Accelerating structure developments for the LEP injector linacs (LIL), in *Proceedings of the 1984 Linear Accelerator Conference, Seeheim, Germany, 1985*, p. FRQ0003.

[38] W. Farabolini, D. Bogard, A. Brabant, A. Curtoni, P. Girardot, F. Gobin, R. Granelli, F. Harrault, C. Lahonde, T. Lerch, M. Luong, A. Mosnier, F. Orsini, F. Peauger, and C. Simon, Diagnostics for the CTF3 probe beam linac CALIFES, in *Proceedings of the 8th European Workshop on Beam Diagnostics and Instrumentation for Particle Accelerators, DIPAC2007, Venice, Italy, 2007*, p. TUPB17.

[39] R. Pan, A. Andersson, W. Farabolini, A. Goldblatt, T. Lefèvre, M. Martyanov, S. Mazzoni, L. Timeo, S. Rey, S. Jamison, W. Gillespie, and D. Walsh, Electro-optical bunch profile measurement at CTF3, in *Proceedings of the 4th International Particle Accelerator Conference, IPAC-2013, Shanghai, China, 2013* (JACoW, Shanghai, China, 2013), p. MOPME077.

[40] C. P. Welsch, H. H. Braun, E. Bravin, R. Corsini, S. Döbert, T. Lefèvre, F. A. Tecker, P. Urschütz, B. Buonomo, O. Coiro, A. Ghigo, and B. Preger, Longitudinal beam profile measurements at CTF3 using a streak camera, J. Instrum. **1**, P09002 (2006).

[41] W. Farabolini, Califes probe beam status, in *International Workshop on Linear Colliders 2010, ECFA-CLIC-ILC Joint Meeting, Geneva, 2010*.

[42] S. Casalbuoni, B. Schmidt, P. Schmüser, V. Arsov, and S. Wesch, Ultrabroadband terahertz source and beamline based on coherent transition radiation, Phys. Rev. ST Accel. Beams **12**, 030705 (2009).

[43] N. Sei and T. Takahashi, First demonstration of coherent Cherenkov radiation matched to circular plane wave, Sci. Rep. **7**, 17440 (2017).